TU Delft

Delft University of Technology

Document Version
Final published version

Citation (APA)
AbuHamra, N., Abunahla, H., Ali, A., Waheed, W., Mahmoud, S. T., AlAzzam, A., & Mohammed, B. (2023). RGO-Based Memristive Sensor for Rapid Hydrogen Detection at Room-Temperature. *IEEE Sensors Journal*, *23*(24), 30093-30101. https://doi.org/10.1109/JSEN.2023.3328869

Important note
To cite this publication, please use the final published version (if applicable).
Please check the document version above.

Copyright
In case the licence states “Dutch Copyright Act (Article 25fa)”, this publication was made available Green Open Access via the TU Delft Institutional Repository pursuant to Dutch Copyright Act (Article 25fa, the Taverne amendment). This provision does not affect copyright ownership.
Unless copyright is transferred by contract or statute, it remains with the copyright holder.

Sharing and reuse
Other than for strictly personal use, it is not permitted to download, forward or distribute the text or part of it, without the consent of the author(s) and/or copyright holder(s), unless the work is under an open content license such as Creative Commons.

Takedown policy
Please contact us and provide details if you believe this document breaches copyrights.
We will remove access to the work immediately and investigate your claim.

This work is downloaded from Delft University of Technology.

Green Open Access added to TU Delft Institutional Repository

'You share, we take care!' - Taverne project

https://www.openaccess.nl/en/you-share-we-take-care

Otherwise as indicated in the copyright section: the publisher is the copyright holder of this work and the author uses the Dutch legislation to make this work public.

rGO-Based Memristive Sensor for Rapid Hydrogen Detection at Room Temperature

Nada Abuhamra, Heba Abunahla, Ashraf Ali, Waqas Waheed, Saleh T. Mahmoud, Anas Alazzam, and Baker Mohammad, *Senior Member, IEEE*

***Abstract*—In recent years, there has been a growing interest in investigating the potential of emerging memristor (MR) devices for gas sensing applications, particularly at room temperature. This article reports on a planar Au/reduced graphene oxide (rGO)/Au memristive hydrogen sensor, fabricated on a cost-effective cyclic olefin copolymer (COC) substrate, and utilizing the rGO green carbon material as its active sensing element. The sensor's performance is evaluated using two different testing modes: conventional chemiresistive testing under a constant voltage bias (CVB) and voltage pulse (VP) modes. The CVB mode demonstrates high repeatability, selectivity, response time, and recovery time, indicating the sensor's reliable gas sensing capabilities. In addition, the VP mode significantly enhances the sensor's relative percentage response, indicating its potential for improved gas sensing performance. To optimize the sensor's response, the impact of hydrogen exposure on the MR resistive switching is studied, revealing that the effect is contingent on the VP amplitude. Specifically, gas-enhanced resistive switching is achieved at lower voltage levels, whereas at higher voltage levels, gas exposure slows down the rate of resistive switching. Consequently, voltage-pulse testing is conducted at two voltage magnitudes, low (2.5 V) and high (4.5 V), and the sensor's response is enhanced from 0.5% under CVB mode to 786% under VP mode.**

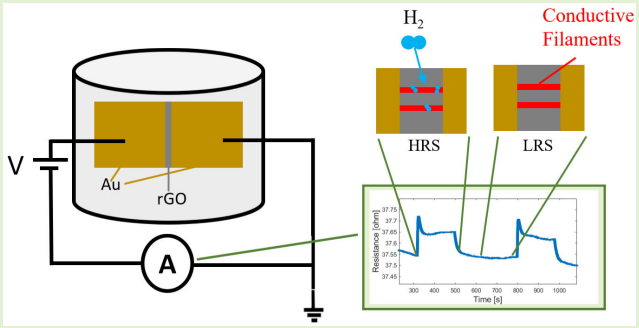

***Index Terms*— Gas sensing, hydrogen sensor, memristor (MR), reduced graphene oxide (rGO).**

I. Introduction

GAS sensing has been a popular topic among the research community, thanks to its wide range of applications in the areas of environmental studies [1], [2], automotive industries [3], [4], indoor air quality supervision [5], [6], and industrial production [7], [8]. Gas sensing methods can be classified into two categories [9]: 1) electrical variations and 2) other variations. The first category (electrical properties variation) includes metal–oxide–semiconductors (MOSs), polymers, carbon nanotubes (CNTs), and moisture-absorbing materials, all of which inherit a change in electrical properties upon exposure to the target gas. The second category (non-electrical variation) includes all the other gas sensing methods like optic, acoustic, calorimetric, and gas chromatography methods [10].

Reliable gas sensors are needed to precisely detect hazardous gases, such as NO_2, H_2S, CO, H_2, and NH_3. Ideal sensors are expected to have high sensitivity, fast response and recovery times, and good selectivity. Different gas sensing methods have different performance indicators; however, they all share the following evaluation metrics [9]: selectivity, sensitivity, response time, recovery time, reversibility, and adsorptive capacity. Other parameters, such as power consumption, weight, size, footprint, fabrication cost, and complexity, are also used to evaluate the overall effectiveness of a gas sensor.

Emerging memristor (MR) devices have been recently explored as a potential candidate for low-power gas sensors

Manuscript received 15 July 2023; revised 27 October 2023; accepted 27 October 2023. Date of publication 6 November 2023; date of current version 14 December 2023. This work was supported by the System-on-Chip Laboratory, Khalifa University, under Award RC2-2018-018. The associate editor coordinating the review of this article and approving it for publication was Prof. Mahesh Kumar. *(Corresponding author: Baker Mohammad.)*

Nada Abuhamra and Baker Mohammad are with the System-on-Chip Center, Electrical Engineering and Computer Science Department, Khalifa University of Science and Technology, Abu Dhabi, UAE (e-mail: 100061115@ku.ac.ae; baker.mohammad@ku.ac.ae).

Heba Abunahla is with the Department of Quantum and Computer Engineering, Delft University of Technology, 2628 CD Delft, The Netherlands (e-mail: h.n.abunahla@tudelft.nl).

Ashraf Ali and Saleh T. Mahmoud are with the Physics Department, United Arab Emirates University, Abu Dhabi, UAE (e-mail: ashraf_ali@uaeu.ac.ae; saleh.thaker@uaeu.ac.ae).

Waqas Waheed and Anas Alazzam are with the System-on-Chip Center, Mechanical Engineering Department, Khalifa University of Science and Technology, Abu Dhabi, UAE (e-mail: waqas.waheed@ku.ac.ae; anas.alazzam@ku.ac.ae).

Digital Object Identifier 10.1109/JSEN.2023.3328869

1558-1748 © 2023 IEEE. Personal use is permitted, but republication/redistribution requires IEEE permission.
See https://www.ieee.org/publications/rights/index.html for more information.

Authorized licensed use limited to: TU Delft Library. Downloaded on January 03,2024 at 08:56:44 UTC from IEEE Xplore. Restrictions apply.

to operate at room temperature [11], [12], [13], [14], [15], [16], [17]. This can be achieved by careful selection of the active sensing layer (typically MOS), along with the device's structure within specific geometries. Moreover, MR devices can form comprehensive systems that are capable of computing, storing, and sensing.

As the name MR implies, MR devices combine the functionality of memories and resistors. To elaborate, the resistance of the MR depends on the applied voltage and the current passing through the device, as well as the device's history or previous state [18]. Such characteristics make MR devices suitable for a wide range of applications, including resistive random access memories [19], transistors [20], artificial neural networks (ANNs) [21], biosensing [22], radiation sensing [23], [24], and gas sensing [11].

To use MR device for gas sensing, the active (sensing) layer must be at least partially exposed to the surrounding air in order for the surface oxidation to take place, affecting the potential barrier and depletion region and therefore allowing for the resistance to change upon exposure to the target gas. The variation in the resistance of MR device occurs due to resistive switching, which is facilitated by the formation and rupturing of conductive filaments in the switching layer that form a low-resistance path for the current to flow between the two electrodes. The resistive switching in MR happens under an applied external electric field, which affects the distribution of oxygen vacancies in valence change memory (VCM) devices and facilitates the ion migration in electrochemical metallization memory (ECM) devices [25]. Having one or more fully formed conductive channels sets the device to a low resistance state (LRS), while rupturing these paths resets the device to a high resistance state (HRS). When MR is exposed to an oxidizing/reducing gas, the stoichiometry of the active layer is changed due to the gas adsorption, affecting the conductive filaments and therefore the resistance of the device.

Different MR-based gas sensors have been reported in the literature [11], [12], [13], [14], [15], [16], [17], [26]. These MR sensors are fabricated with different oxide sensing materials: TiO_2 [11], [12], [13], [26], SnO_2 [15], [17], HfO_2 [15], Ta_2O_5 [15], CuO [16], [27], and Zr_3N_4 [14], for the detection of the H_2 [11], [12], [26], C_2H_6 [15], NO [14], [15], [26], O_2 [16], [27], NH_3 [13], and C_3H_8O [17] gases. Employing different sensing materials in a memristive structure allows the sensors to operate effectively at room temperature, which is a challenge often associated with most MOS-based gas sensors [9].

Another hurdle for MOS-based gas sensors is the long recovery time, which worsens as the target gas concentration increases since more gas molecules need to desorb from the oxide to achieve recovery. To overcome the slow recovery time, Lee et al. proposed the application of an external voltage bias or voltage pulse (VP) across the MR sensor [15]. This enhanced recovery mode improved the recovery time of their SnO_2-based MR H_2 sensor from 700 to 27 s with the help of a voltage bias, and to 90 ns with the help of an applied VP. The enhanced recovery mode was also tested in [14]. For their Zr_3N_4-based MR NO sensor, where the application of an external VP reduced the recovery time to 1 s.

Vidiš et al. [11] proposed the gasistor (gas-triggered switch) application of MR gas sensors. To operate their TiO_2-based MR H_2 gas sensor as a gasistor, the sensor was exposed to a constant flow of 10 000 ppm of H_2 gas while biased with a constant current bias. During hydrogen gas exposure, the voltage induced by the current source was lower than the MR's V_{set}, and the resistance of the MR was constant. Upon shutting-off the H_2 gas flow, the device recovered to its initial resistance state. In other words, the resistance of the device is increased, and therefore, the voltage induced by the current source is increased and surpassed V_{set}. Therefore, the MR switched from the HRS to LRS as a response to the applied voltage by the current source, which increased due to the absence of the H_2 gas. Qiu et al. [13] also tested the gas-triggered switch functionality with their TiO_2-based MR NH_3 sensor. The gasistor functionality was realized by maintaining the flow of NH_3 gas at a constant concentration under a constant current bias. The flow of gas was then shut-off which triggered the MR to switch from the HRS to LRS thanks to the higher induced voltage by the current source.

This article aims to advance gas sensing technology using MR sensors. Specifically, the proposed MR-based sensor targets the highly flammable H_2 gas at room temperature. The active material used in this work is a sustainable 2-D carbonaceous material: reduced graphene oxide (rGO). Other carbonaceous materials have been studied for room-temperature gas sensing, such as graphene, CNTs, and activated carbon (AC) beads [28], [29]. Different low-dimensional nanomaterials have been reported for various sensing applications, such as pressure sensing [30], [31], humidity sensing [32], [33], and gas sensing [34], [35], all thanks to their intrinsic characteristics, such as the high surface area, tunable electrical conductivity, surface functionalization, and chemical sensitivity.

The rest of this article is organized as follows. Section II provides a detailed description of the fabrication process, material characterization, and electrical characterization of a new deployment of rGO-based MR device for H_2 gas sensing. Next in Section III, this article presents the testing results of the proposed rGO-based MR sensor for H_2 gas at room temperature under two modes of operation, demonstrating the sensor's selectivity, repeatability, and fast response. In Section IV, the possible sensing mechanism is explained. Finally, Section V concludes this article by summarizing the key findings and highlighting the significance of the research in the field of gas sensing using MR technology.

II. Proposed Device Fabrication and Electrical Characterization

To be able to use graphene oxide (GO) for gas sensing, the film must be electrically conductive enough, which in the case of rGO is achieved via reduction of GO. It should also be kept in mind that the device must fully recover to its LRS before each test to get reproducible results [36]. When it comes to the MR device structure, the planar option makes the most sense for sensing applications as the active sensing layer has a relatively large surface area that allows for the direct interaction between the gas and the sensing layer.

Authorized licensed use limited to: TU Delft Library. Downloaded on January 03,2024 at 08:56:44 UTC from IEEE Xplore. Restrictions apply.

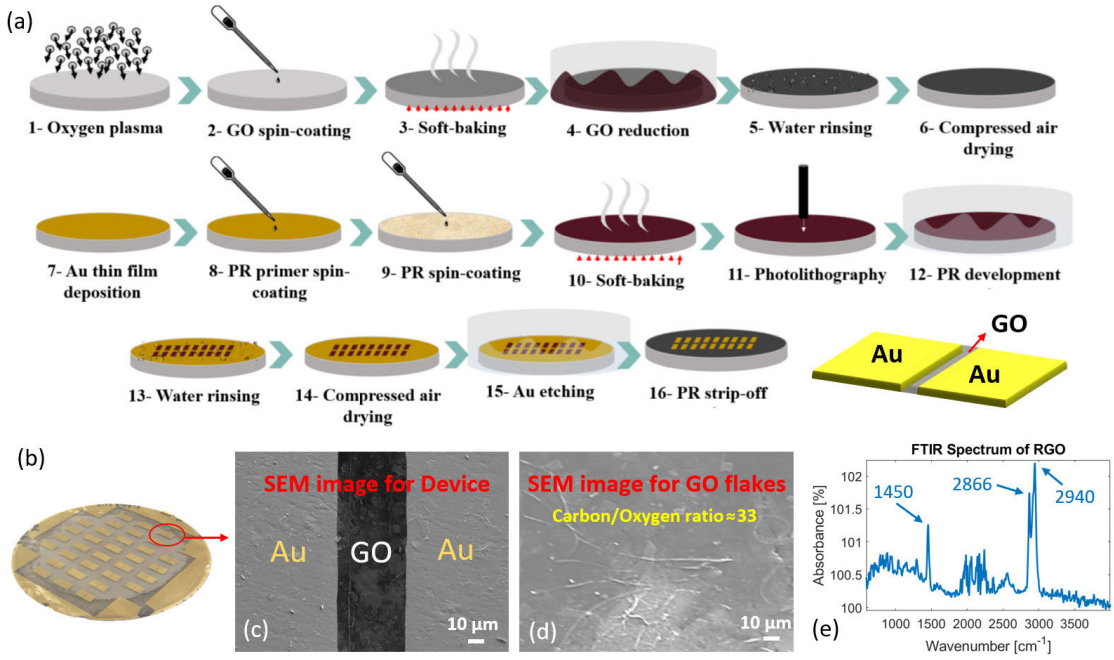

Fig. 1. Proposed planar Au/rGO/Au memristive hydrogen sensor on a COC wafer. (a) Fabrication steps schematic. (b) Photograph for the fabricated devices. (c) SEM image of a single fabricated device. (d) SEM-EDX image of rGO flakes, with carbon/oxygen ratio of 33. (e) FTIR absorbance spectrum of rGO.

The stacked MR device architecture has been studied for gas sensing applications and has shown the ability to operate at room temperature within specific geometries as reported in [11]. However, due to the potential advantages of having a larger specific surface area in contact with the gas, this study focuses on exploring the gas sensing capabilities of the planar MR device architecture at room temperature.

Furthermore, the sensor proposed in this work has inert gold (Au) electrodes with a film of rGO as the sensing material. RGO is deployed as the sensing element in the proposed memristive sensor to overcome the high temperature requirement. The Au/rGO/Au architecture was realized before in the literature [37] and studied for the multiply accumulate (MAC) operation that is crucial for artificial neural networks (ANNs) as the device is capable of analog switching and mimics the functionality of a synapse. Moreover, one of the proposed applications for these NeuroMem devices was gas sensing as the rGO has a large surface area. Thus, in the scope of this work, the planar Au/rGO/Au system is studied for room temperature H_2 gas.

The planar architecture of the device with the same electrode material reduces the fabrication steps when compared with stacked devices or even other planar devices with two different electrode materials. This reduces the fabrication complexity and, therefore, the fabrication cost. Moreover, the utilization of a cyclic olefin copolymer (COC) substrate provides a cost-effective medium that allows for improved wettability when treated with oxygen plasma, enhancing the adhesion of GO to the substrate [38]. These devices are fabricated by a standard microfabrication process, where the rGO films, deposited between the two Au electrodes, are synthesized from an aqueous solution of GO and ethanol.

The fabrication process starts with cleaning a COC wafer with ethanol and isopropanol, drying it with compressed air, and then baking it. After that, the COC wafer undergoes surface activation with oxygen plasma for 5 min to enhance the adhesion of GO on the substrate [39]. Next, the prepared GO solution is spin coated on the wafer at a speed of 1000 r/min. The wafer is then baked on a hot plate at 70 °C for 2 min to dry the GO layer by evaporating the solvents. The GO spin-coating and baking is repeated four times to get the required GO layer thickness. The GO layer is then reduced to rGO by submerging the wafer in Hydriodic acid for 10 min. The effect of reduction time on the film's electrical resistivity has been discussed in our previous work [40]. Next, a thin gold film (40 nm) is deposited on the wafer using a thermal evaporator at 1E − 7 mbar pressure with a tooling factor of 100% and a sensor rate of 0.25 Å/s. After the gold deposition, a photoresist primer, hexamethyldisilazane (HMDS), is spin-coated on the wafer at 4000 r/min, followed by the spin-coating of a positive photoresist (Microposit S1813) on the wafer at 4000 r/min. The wafer is then baked at 70 °C for 3–5 min to evaporate the solvents from the photoresist. Next, the (3 × 3 mm) gold electrodes patterning with a gap of 50 μm is done by photolithography using KLOE 650 maskless photolithography system. After UV exposure, the photoresist is developed for 1 min in MF319 developer and the wafer is then rinsed with water. After the photoresist development, a gold etchant is used to remove exposed metal areas. Finally, acetone is used to strip-off the remaining (unexposed) photoresist leaving underneath it the protected gold electrodes. A schematic of the fabrication steps is shown in Fig. 1(a). Device image, SEM image, and SEM-EDX analysis of GO flakes are shown in Fig. 1(b)–(d). The obtained carbon/oxygen ratio reflects the partial reduction of GO. The absorbance spectrum obtained

Authorized licensed use limited to: TU Delft Library. Downloaded on January 03,2024 at 08:56:44 UTC from IEEE Xplore. Restrictions apply.

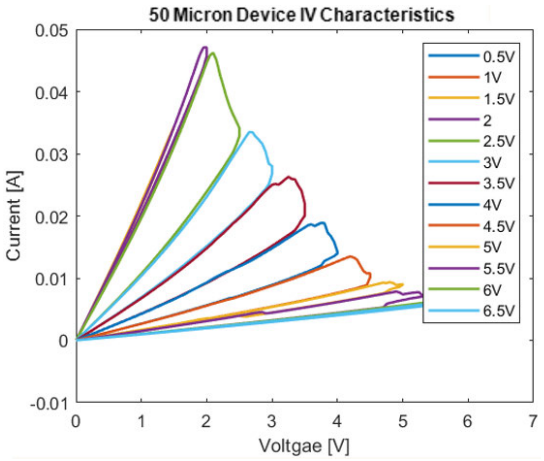

Fig. 2. Fabricated memristor's *I–V* characteristics with a voltage step of 0.5 V.

from Fourier transform infrared (FTIR) analysis in Fig. 1(e) supports the SEM-EDX results. To elaborate, missing oxygen-functional groups' peaks, such as the broad peak between 3000 and 3600 cm^{-1} corresponding to O–H vibration, indicate the effective reduction of GO [41]. Moreover, peaks at 2941 and 2864 cm^{-1} are due to CH_2 asymmetric and symmetric stretching of GO [42], and the peak at 1450 cm^{-1} corresponds to C–H bending mode [43].

The detailed electrical characterization of the Au/rGO/Au MR devices was done in our previous work [37]. The device shows its analog switching capability, where the new state written on the device is a function of the applied voltage as well as the previous state. Moreover, the device shows unipolar switching depicted by the symmetric *I–V* characteristics obtained for the same voltage magnitude at opposite polarities. It is worth mentioning that these devices are found in the LRS in their pristine state and are switched to higher resistance states with the application of a voltage bias. The higher the supplied voltage level, the higher the resistance state written on the device, and the higher the required voltage for the next write operation. Fig. 2 shows 13 voltage sweeps across a pristine Au/rGO/Au device, with a voltage step of 0.5 V, highlighting the device's capability of writing multiple resistance states. This behavior is explained by the Joule heating phenomena, where a specific heating power is to be reached for the resistive switching to occur. With increased resistance, the current is reduced; therefore, a higher voltage is required to reach the heating power that switches the device to a new resistance state [37].

III. Gas Sensing Experiments and Discussion

To study the sensor's response to hydrogen gas exposure, several gas sensing tests were carried out at room temperature and 0% relative humidity (RH) using the setup shown in Fig. 3, where the flow of gas is controlled by a mass flow controller (MFC) and measurements are recorded using a Keithley source meter. For real-time gas monitoring, a portable platform similar to the one developed in [44] can be utilized to measure the sensor signal. The proposed sensor is tested under two different operation modes: conventional chemiresistive

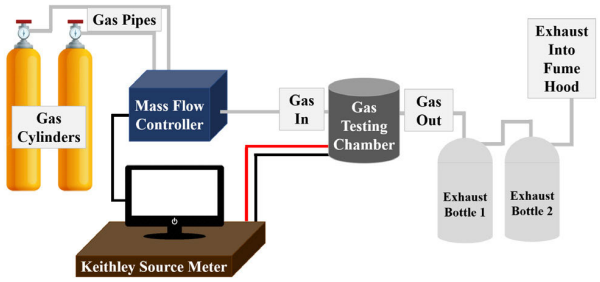

Fig. 3. Schematic of the gas sensing experimental setup.

testing under a constant voltage bias (CVB) and VP mode. Since the synthesized devices are symmetric, either one of the electrodes is connected to the voltage bias, and the other is grounded, as shown in Fig. 4(a). Prior to gas sensing tests, device stability is assessed in normal air atmosphere at room temperature under the application of the bias voltage. Long-term stability testing is demonstrated over a 72-h period, confirming the device's long-term stability as plotted in Fig. 4(a).

A. CVB Mode Results

The results provided in Fig. 4(b) show the sensor's resistance versus time for two separate gas sensing runs under the voltage bias of 0.7 and 1.3 V. Each test sequence starts with 315 s of nitrogen flushing at 200 standard cubic centimeters per minute (SCCM), after which, 1000 ppm of hydrogen is introduced to the chamber for 180 s. The chamber is then rinsed again with 200 SCCM of nitrogen for 300 s, and the hydrogen sequence is repeated and followed by a 5-min nitrogen flush. The sensor shows a rapid response to the hydrogen gas depicted by the rapid increase in sensor resistance. It is worth noting that the response of the sensor is higher under the 1.3-V bias compared with the 0.7-V bias. Thus, to study the effect of the voltage bias on the device's sensing performance, the same testing sequence is repeated on the same device at different bias voltages in the range of (0.5–1.2) V, and the response is found to be highly repeatable with a distinct profile as shown in Fig. 4(c) and (d). The trend shows a positive relation between the bias voltage and the sensor response, where increasing the bias voltage by 2.4 times (0.5–1.2 V) increased the relative percentage response by 2.5 times (0.19%–0.48%). This result suggests that the sensor's response is due to the synergistic effect of the gas interaction with the oxide layer and the applied voltage across the device. The changes in resistance show resistive switching to a higher resistance value as a response to the hydrogen gas exposure. Moreover, the resistance plot of the sensor portrays its ability to recover to its initial state, which is not possible when switched electrically. Fig. 4(e) shows the sensor's relative percentage response $[(R_{air} - R_{gas})/(R_{air}) \times 100]$ toward different concentrations of H_2 at room temperature.

To study the effect of the rGO layer width on the performance of the sensors, three device variations are fabricated with rGO widths of 50, 100, and 150 μm. All three device variations show the same electrical characteristics with slight variations. To elaborate, these devices are found in the LRS state in their pristine state and with a large enough applied

Authorized licensed use limited to: TU Delft Library. Downloaded on January 03,2024 at 08:56:44 UTC from IEEE Xplore. Restrictions apply.

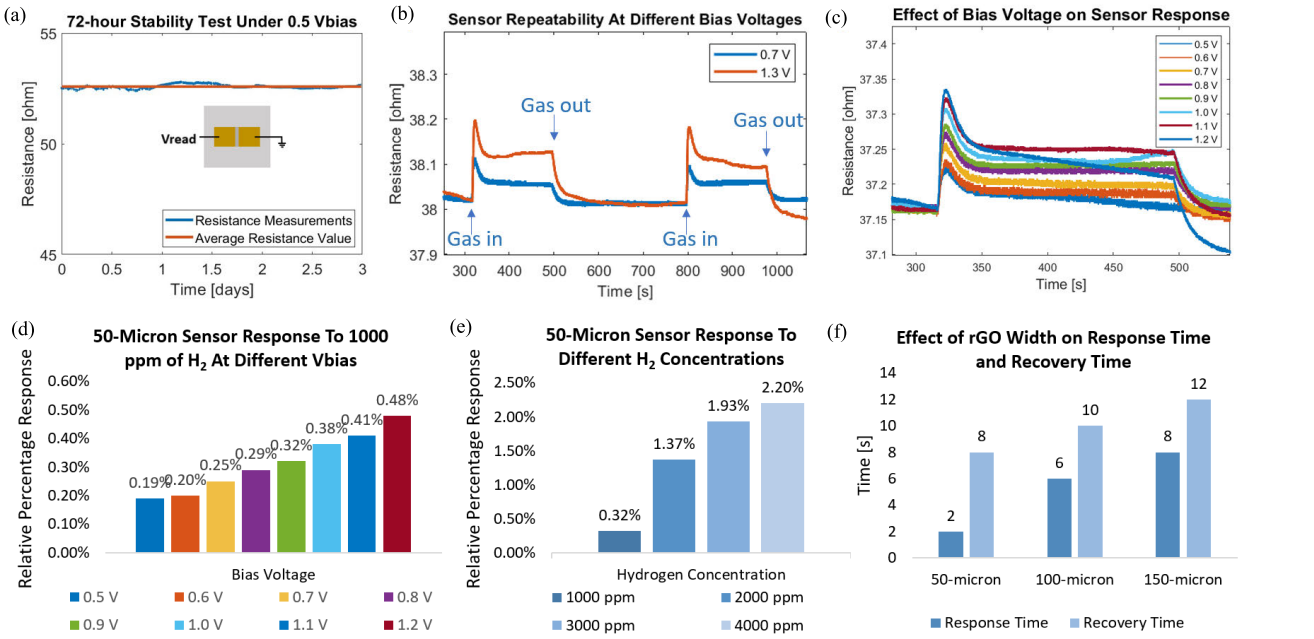

Fig. 4. (a) Long-term stability test, (b) sensor response to 1000 ppm of hydrogen at room temperature and 0% RH, (c) and (d) effect of bias voltage on the sensor response to 1000 ppm of hydrogen, (e) response of sensor to different concentrations of hydrogen, and (f) effect of rGO layer width on response and recovery times of sensors toward 1000 ppm of hydrogen. All tests were conducted at room temperature and 0% RH.

voltage, and the devices switch to a higher resistance state until they reach the HRS. The voltage required to trigger resistive switching is proportional to the width of the rGO layer, where the minimum trigger voltage for the 50, 100, and 150-μm MRs is found to be 2, 2.5, and 3.5 V, respectively. Moreover, the I–V curves of all three devices show pinched hysteresis, a fingerprint of MRs that highlights both their memory and resistive behavior. While no correlation is found between the sensor's relative percentage response and the width of the rGO layer, the response and recovery times increase as the width of the sensing layer increases, as shown in Fig. 4(f).

To ensure the sensor's selectivity toward hydrogen gas, the resistance of the device is monitored, and the response is calculated toward 1000 ppm of five gases, namely, H_2, H_2S, CO_2, CO, and C_2H_4. Each test is repeated for 2 cycles of 3-min gas exposure. Fig. 5 shows the comparison of the response of the sensor toward 1000 ppm of multiple gases at room temperature and 0% RH. Not only the sensor found to be highly selective toward hydrogen, but the immediate sensor response and recovery are also only evident for the H_2 gas.

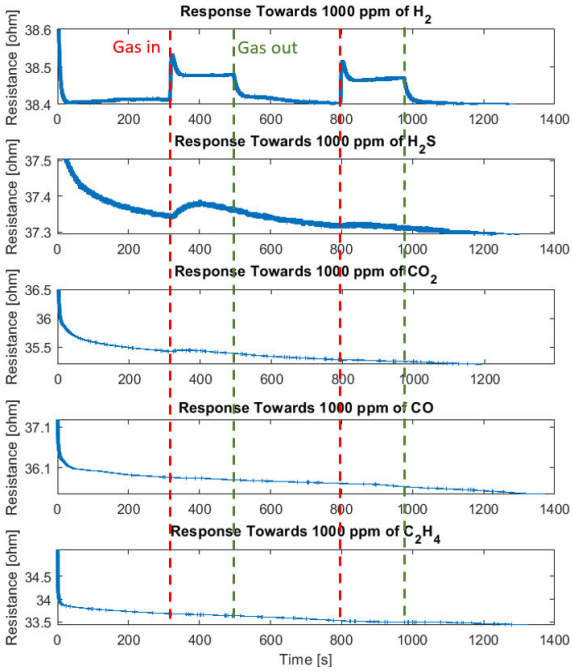

Fig. 5. Selectivity test data on MR hydrogen sensor toward 1000 ppm of H_2, H_2S, CO_2, CO, and C_2H_4 at room temperature and 0% RH.

B. PV Mode Results

To study the effect of hydrogen exposure on the MR's resistive switching, a voltage sweeping test is carried out on two 50-μm devices, a control device (normal atmosphere) and a sense device (1000 ppm of H_2). The 11 I–V curves are acquired from both devices at room temperature starting at 0.5 V with a step of 0.5 V between each two consecutive sweeps as plotted in Fig. 6(a). The first two sweeps show pure ohmic behavior for both devices. The next sweeps show nonlinearity, where the resistance of both devices decreases by 6.9% in the third sweep and by 12.6% in the fourth sweep. The fifth sweep (0–2.5 V) is where the difference between the two devices becomes visible. The sense device shows its first resistive switch from 34.47 to 44.48 Ω, while the control device shows nonlinearity without signs of resistive switching. In the sixth sweep, where the switching voltage is surpassed, both devices switch to a higher resistance state. After that sweep, the control device switches to higher resistance states at a much higher rate compared with that of the sense device. After the seventh sweep, the control device shows no further switching, which means that any variations in the control device's resistance is completely due to the nonlinearity of the device and not due to triggered resistive switching.

Authorized licensed use limited to: TU Delft Library. Downloaded on January 03,2024 at 08:56:44 UTC from IEEE Xplore. Restrictions apply.

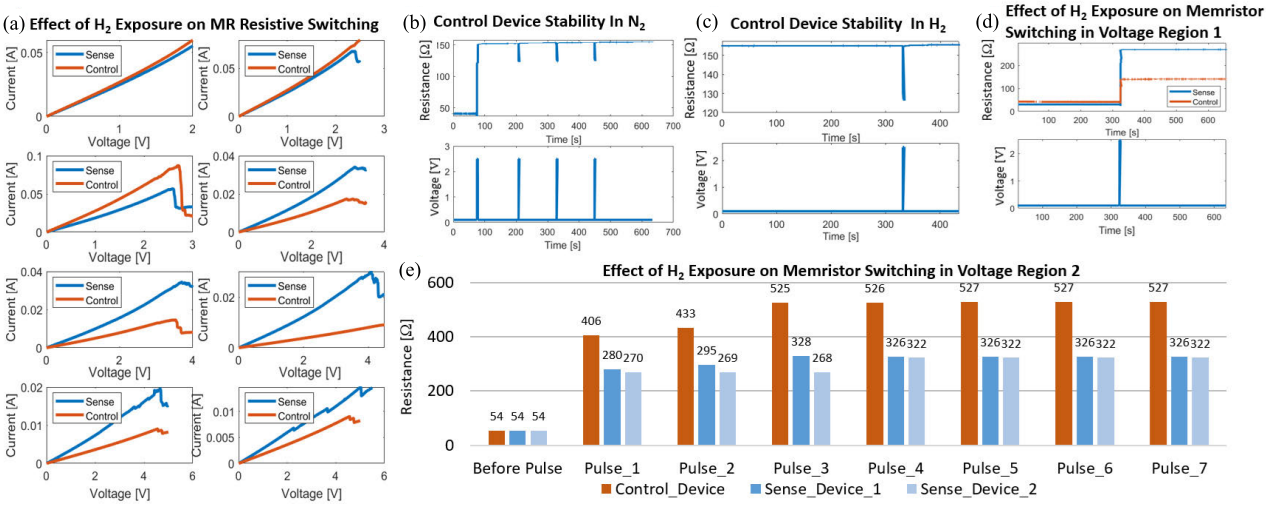

Fig. 6. (a) *I–V* characteristics of control (normal atmosphere) and sense (1000-ppm H_2) devices. Resistance of control device in nitrogen atmosphere after the application of 2.5-V pulses in (b) nitrogen atmosphere and (c) 1000 ppm of hydrogen, (d) difference in resistance between control device in nitrogen and sense device in 1000 ppm of hydrogen after the application of a 2.5-V pulse, and (e) resistance of a control device and two sensors after the application of seven 4.5-V pulses. All data were acquired at room temperature and 0% RH.

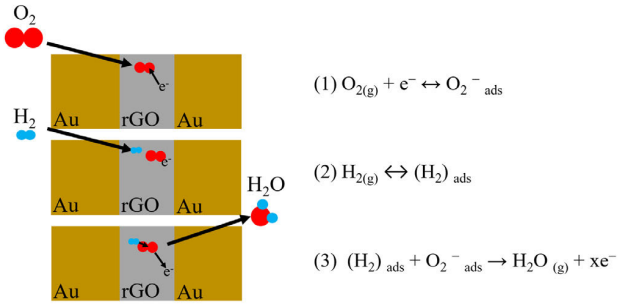

Fig. 7. Possible sensing mechanism.

TABLE I
PERFORMANCE COMPARISON OF rGO-BASED HYDROGEN SENSORS

H_2 Concentration	Response Time	Recovery Time	Operating Temperature	Ref
400 ppm	12 s	412 s	100 °C	[34]
10,000 ppm	28 s	142 s	50 °C	[35]
100 ppm	45 s	27 s	150 °C	[46]
1,000 ppm	18 s	39 s	Room temperature	[47]
500 ppm	-	-	250 °C	[48]
200 ppm	1 s	12 s	300 °C	[49]
500 ppm	18 s	29 s	180 °C	[50]
1,000 ppm	2 s	8 s	Room temperature	This work

By conducting the sweep test, it can be concluded that the overall effect of the H_2 gas exposure on the resistive switching of the MR-based sensor is divided into three regions: 1) before trigger voltage (0–2 V); 2) after trigger voltage (2–4 V); and 3) after switch-off voltage (4–5.5 V). In the first voltage region, where the trigger voltage is not yet reached, the sense device shows higher resistance readings and advanced resistive switching. In the second voltage region, where the trigger voltage is reached as evident by the resistive switching of the control device, the sense device shows denoted switching compared with the control device. In the third and final voltage region, where the switch off voltage is surpassed, the sense device is still capable of resistive switching as evident in the last three sweeps, while the control device is not. Thus, it is concluded that the hydrogen gas exposure advances the resistive switching, as evident by the lower trigger voltage, and slows down the switching rate, as evident by the lower change in resistance.

The next gas sensing test is designed to take advantage of the voltage-enhanced resistive switching in voltage region 1 (below trigger voltage). First, the stability of the control device is tested in nitrogen atmosphere and then in 1000-ppm H_2, as illustrated in Fig. 6(b) and (c). Next, a 3-s VP of 2.5 V is applied across two fresh devices, a control and a sense device. As expected from the sweep test, the sense device switched to a higher resistance state (270 Ω) compared with the control device (140 Ω) as plotted in Fig. 6(d). This sensing approach enhances the sensor response to 1000 ppm of hydrogen at RT and 0% RH from 0.48% at a CVB of 1.2 V to 785.75% with a VP of 2.5 V for 3 s. The drawback with this method, however, is that the sensing is not reversible, and therefore, the device under this operation mode is considered a single-use device. However, considering the simple fabrication process, compact device size, and cost-effectiveness of rGO, an array of sensors can be fabricated such that the number of devices depicts the number of possible sensing instances.

The enhanced response captured from the VP mode suggests that this mode of operation is worth exploring even if it yields single-use sensors. Accordingly, the next gas sensing test is conducted using the VP mode in the second voltage region (4.5 V), where the resistance of the sense device is expected to be lower than that of the control device because of the slower switching rate caused by hydrogen exposure. Multiple 3-s VPs are applied across fresh 100-μm devices, and the resistance after each pulse is recorded and plotted in Fig. 6(e). As expected, the control device switched to a higher resistance state is compared with the sense devices. It is worth noting that even though it took the devices 3–4 pulses to saturate, the measurements from the control device, even before saturation, were considerably higher than those of the sense devices, hence, the detection of gas is possible after the very first VP.

Authorized licensed use limited to: TU Delft Library. Downloaded on January 03,2024 at 08:56:44 UTC from IEEE Xplore. Restrictions apply.

TABLE II
PERFORMANCE COMPARISON OF MR-BASED HYDROGEN SENSORS

Materials	H_2 Concentration	Response Time	Recovery Time	Operating Temperature	Selectivity (demonstrated towards H_2 against)	Ref
Pt/TiO_2/Pt	10,000 ppm	100 s	-	Room Temperature	-	[11]
Pt/TiO_2/Pt	10,000 ppm	35 s	180 s	Room Temperature	CO, NO_2	[12]
Pt/TiO_2/TiN	10,000 ppm	200 s	5 s	Room Temperature	-	[26]
Au/rGO/Au	1,000 ppm	2 s	8 s	Room Temperature	H_2S, CO, CO_2, C_2H_4	This work

C. Sensor Performance Comparison

To demonstrate the satisfactory performance of the proposed Au/rGO/Au MR-based H_2 sensor, the device performance is compared with other rGO-based H_2 sensors in Table I. The general trend in the transient response versus concentration for all gas sensors is that the response time is quicker for higher concentrations, and that the recovery time is slower. This is because with higher concentrations, more time is required for the gas molecules to desorb from the sensing material to achieve recovery. Moreover, rGO-based H_2 sensors typically do not operate effectively at room temperature as evident from Table I. Thus, integrating rGO as the sensing material in an MR structure facilitated its room temperature operation in the proposed sensor device. The references in Table I show that, generally, for lower concentrations of hydrogen gas, the operating temperatures of the sensors must be elevated, while for higher concentrations of hydrogen, a relatively lower operating temperature is sufficient for sensing. Compared with other rGO-based hydrogen sensors, both the response and recovery of the proposed sensor are among the highest (2 and 8 s, respectively).

The proposed sensor's performance is also compared to other MR-based H_2 sensors in Table II. All the other reported sensors [11], [12], [26] used TiO_2 as the sensing element, and Pt or TiN as electrode materials. Interestingly, all the reported MR-based H_2 sensors, including the one proposed in this work, report sensing at room temperature, which highlights one of the potential benefits of deploying sensitive semiconductors in memristive gas sensors to overcome high-operating temperature requirements. Compared with the references in Table II, the reported Au/rGO/Au sensor exhibits quick response/recovery times and demonstrates excellent selectivity toward H_2 compared with other gases.

IV. GAS SENSING MECHANISM

Gas sensing using semiconductive materials is carried out in two stages, the first of which is through redox reactions, where target gas molecules react with the negative adsorbed oxygen ions. This reaction is then transduced into an electrical variation in the sensor's resistivity [45]. In the proposed Au/rGO/Au device, the electrical resistance of the sensor increases upon exposure to the target gas (hydrogen), showing p-type behavior from the rGO sensing layer. A possible explanation for this phenomenon is due to the redox reactions between the hydrogen molecules and the rGO sensing layer. Hydrogen is a reducing gas, which means that it interacts with the rGO film by capturing the negative adsorbed oxygen species. This reaction results in releasing the electrons trapped by the oxygen anions back into the p-type semiconductor, which results in increasing the potential barrier and therefore increasing the electrical resistance. This increase in resistance writes the MR to a new HRS. SEM-EDX analysis performed on the device in PV mode prior to and after exposure to H_2 revealed the decrease in oxygen content after exposure to H_2S, supporting this sensing mechanism. After exposure to the hydrogen gas, the resistance of the device is reduced back to its initial resistance state, which can be understood by the absence (desorption) of hydrogen gas, and the presence of oxygen in the surrounding air. The interaction between hydrogen and rGO can be summarized by the chemical equations in Fig. 7 [35], [46]. The first step includes the formation of negatively charged adsorbed oxygen species ($O^-_{2\ ads}$) on the surface of rGO. The adsorption occurs by oxygen molecules capturing electrons from the rGO surface. The second step shows the adsorption of hydrogen gas molecules on the surface of rGO. This step could rupture the conductive filaments of MR [14]. The final step involves the chemical reaction between the adsorbed hydrogen molecules and the adsorbed oxygen anions to form water vapor and release some of the captured electrons back into the material. These chemical reactions change the stoichiometry of the rGO layer, which translates into electrical resistance changes that are evident upon exposure to the target gas.

V. CONCLUSION

This work presents a novel approach to gas sensing by investigating the potential of planar memristive devices as H_2 gas sensors, using a planar rGO-based MR sensor. The novelty of this work lies in its high sensitivity and selectivity, as well as the use of simple fabrication processes. Upon testing the fabricated devices in the conventional chemiresistive testing scheme under the CVB mode, the devices showed stability, selectivity toward hydrogen, high repeatability, quick response and recovery times, and operation at room temperature. Although the response of the proposed sensor was highly repeatable, it was initially relatively low. To optimize the sensor's response, the memristive nature of the fabricated devices was leveraged. Instead of applying a small CVB, a VP was repeatedly applied across the device to take advantage of the MR's resistive switching capability. Specifically, much higher responses were observed upon testing the fabricated

Authorized licensed use limited to: TU Delft Library. Downloaded on January 03,2024 at 08:56:44 UTC from IEEE Xplore. Restrictions apply.

devices under the VP mode due to the gas-enhanced/gas-denoted resistive switching. One drawback of the VP operation mode, however, is the single-use nature of the devices and the need for a control device. Nonetheless, these results demonstrate the potential for improving the performance of memristive-based gas sensors using pulse voltage techniques. With the proper design of the MR-based sensor and careful selection of the sensing layer, the proposed MR sensor has outperformed other rGO-based H_2 sensors by achieving H_2 gas sensing at room temperature. While MR is a relatively new technology for gas sensing, with its promising sensing capabilities, it might take the lead in the future of gas sensing.

REFERENCES

[1] G. F. Fine, L. M. Cavanagh, A. Afonja, and R. Binions, "Metal oxide semi-conductor gas sensors in environmental monitoring," *Sensors*, vol. 10, no. 6, pp. 5469–5502, Jun. 2010.

[2] Y. Su et al., "Maxwell displacement current induced wireless self-powered gas sensor array," *Mater. Today Phys.*, vol. 30, Jan. 2023, Art. no. 100951.

[3] M. Soufian et al., "Real-time emission monitoring and display to reduce vehicle pollution using wireless network," in *Proc. 12th Int. Conf. Develop. eSystems Eng. (DeSE)*, Oct. 2019, pp. 960–963.

[4] I. Marr, S. Reiß, G. Hagen, and R. Moos, "Planar zeolite film-based potentiometric gas sensors manufactured by a combined thick-film and electroplating technique," *Sensors*, vol. 11, no. 8, pp. 7736–7748, Aug. 2011.

[5] G. Xiao et al., "Trace amount formaldehyde gas detection for indoor air quality monitoring," in *Proc. IEEE Int. Instrum. Meas. Technol. Conf.*, May 2011, pp. 1–4.

[6] J. Courbat et al., "Ultra-low power metal-oxide gas sensor on plastic foil," in *Proc. TRANSDUCERS Int. Solid-State Sensors, Actuat. Microsystems Conf.*, 2009, pp. 584–587.

[7] A. Ayes et al., "Enhanced hydrogen gas detection using SAW sensor through oxygen pre-treatment," in *Proc. IEEE Int. Ultrason. Symp. (IUS)*, Oct. 2019, pp. 189–192.

[8] L. Klein et al., "Wireless sensor networks for fugitive methane emissions monitoring in oil and gas industry," in *Proc. IEEE Int. Congr. Internet Things (ICIOT)*, Jul. 2018, pp. 41–48.

[9] X. Liu, S. Cheng, H. Liu, S. Hu, D. Zhang, and H. Ning, "A survey on gas sensing technology," *Sensors*, vol. 12, no. 7, pp. 9635–9665, Jul. 2012.

[10] S. Mahajan and S. Jagtap, "Metal-oxide semiconductors for carbon monoxide (CO) gas sensing: A review," *Appl. Mater. Today*, vol. 18, Mar. 2020, Art. no. 100483.

[11] M. Vidiš et al., "Gasistor: A memristor based gas-triggered switch and gas sensor with memory," *Appl. Phys. Lett.*, vol. 115, no. 9, Aug. 2019, Art. no. 093504.

[12] A. A. Haidry, A. Ebach-Stahl, and B. Saruhan, "Effect of Pt/TiO_2 interface on room temperature hydrogen sensing performance of memristor type Pt/TiO_2/Pt structure," *Sens. Actuators B, Chem.*, vol. 253, pp. 1043–1054, Dec. 2017.

[13] P. Qiu, Y. Qin, and Q. Xia, "Ultrasensitive memristor-based gas sensor (gasistor) with gas-triggered switch and memory function for dilute NH_3 detection," *Sens. Actuators B, Chem.*, vol. 373, Dec. 2022, Art. no. 132730.

[14] D. Lee, J. Jung, S. Kim, and H.-D. Kim, "Gas detection and recovery characteristics at room temperature observed in a Zr_3N_4-based memristor sensor array," *Sens. Actuators B, Chem.*, vol. 376, Feb. 2023, Art. no. 132993.

[15] D. Lee, M. J. Yun, K. H. Kim, S. Kim, and H.-D. Kim, "Advanced recovery and high-sensitive properties of memristor-based gas sensor devices operated at room temperature," *ACS Sensors*, vol. 6, no. 11, pp. 4217–4224, Nov. 2021.

[16] C. Nyenke and L. Dong, "Sensing ambient oxygen using a W/CuxO/Cu memristor," in *Proc. 10th IEEE Int. Conf. Nano/Micro Engineered Mol. Syst.*, Apr. 2015, pp. 254–258.

[17] D. Lee, D. Bae, M. Chae, and H.-D. Kim, "High sensitivity of isopropyl alcohol gas sensor based on memristor device operated at room temperature," *J. Korean Phys. Soc.*, vol. 80, no. 11, pp. 1065–1070, Jun. 2022.

[18] S. Carrara, "The birth of a new field: Memristive sensors. A review," *IEEE Sensors J.*, vol. 21, no. 11, pp. 12370–12378, Jun. 2021.

[19] D. Sacchetto, M. Zervas, Y. Temiz, G. De Micheli, and Y. Leblebici, "Resistive programmable through-silicon vias for reconfigurable 3-D fabrics," *IEEE Trans. Nanotechnol.*, vol. 11, no. 1, pp. 8–11, Jan. 2012.

[20] D. Sacchetto, M. H. Ben-Jamaa, S. Carrara, G. De Micheli, and Y. Leblebici, "Memristive devices fabricated with silicon nanowire Schottky barrier transistors," in *Proc. IEEE Int. Symp. Circuits Syst.*, May 2010, pp. 9–12.

[21] T. Wang, H. Huang, X. Wang, and X. Guo, "An artificial olfactory inference system based on memristive devices," *InfoMat*, vol. 3, no. 7, pp. 804–813, Jul. 2021.

[22] H. Abunahla et al., "MOMSense: Metal-oxide-metal elementary glucose sensor," *Sci. Rep.*, vol. 9, no. 1, p. 5524, Apr. 2019.

[23] H. Abunahla et al., "MemSens: Memristor-based radiation sensor," *IEEE Sensors J.*, vol. 18, no. 8, pp. 3198–3205, Apr. 2018.

[24] H. Abunahla et al., "Synthesis and Characterization of micro-thick TiO_2 and HfO_2 memristors," in *Memristor Technology: Synthesis and Modeling for Sensing and Security Applications* (Analog Circuits and Signal Processing). Springer, 2018, pp. 31–51. [Online]. Available: https://link.springer.com/chapter/10.1007/978-3-319-65699-1_2#citeas

[25] B. Mohammad et al., "State of the art of metal oxide memristor devices," *Nanotechnol. Rev.*, vol. 5, no. 3, pp. 311–329, Jan. 2016.

[26] S. Y. Chun et al., "An artificial olfactory system based on a chemi-memristive device," *Adv. Mater.*, vol. 35, no. 35, Sep. 2023, Art. no. 2370251.

[27] C. Nyenke and L. Dong, "Fabrication of a W/CuxO/Cu memristor with sub-micron holes for passive sensing of oxygen," *Microelectronic Eng.*, vol. 164, pp. 48–52, Oct. 2016.

[28] M. H. Zarifi, M. Fayaz, J. Goldthorp, M. Abdolrazzaghi, Z. Hashisho, and M. Daneshmand, "Microbead-assisted high resolution microwave planar ring resonator for organic-vapor sensing," *Appl. Phys. Lett.*, vol. 106, no. 6, Feb. 2015, Art. no. 062903.

[29] M. Fayaz et al., "Monitoring the residual capacity of activated carbon in an emission abatement system using a non-contact, high resolution microwave resonator sensor," *Sens. Actuators B, Chem.*, vol. 282, pp. 218–224, Mar. 2019.

[30] H. Pan et al., "Biodegradable cotton fiber-based piezoresistive textiles for wearable biomonitoring," *Biosensors Bioelectron.*, vol. 222, Feb. 2023, Art. no. 114999.

[31] Y. Su et al., "High-performance piezoelectric composites via β phase programming," *Nature Commun.*, vol. 13, no. 1, p. 4867, Aug. 2022.

[32] C. Chen et al., "Ni-Co-P hollow nanobricks enabled humidity sensor for respiratory analysis and human-machine interfacing," *Sens. Actuators B, Chem.*, vol. 370, Nov. 2022, Art. no. 132441.

[33] Y. Su et al., "Sensing–transducing coupled piezoelectric textiles for self-powered humidity detection and wearable biomonitoring," *Mater. Horizons*, vol. 10, no. 3, pp. 842–851, 2023.

[34] Q. A. Drmosh et al., "A novel approach to fabricating a ternary rGO/ZnO/Pt system for high-performance hydrogen sensor at low operating temperatures," *Appl. Surf. Sci.*, vol. 464, pp. 616–626, Jan. 2019.

[35] H. Ren, C. Gu, S. W. Joo, J. Zhao, Y. Sun, and J. Huang, "Effective hydrogen gas sensor based on NiO@rGO nanocomposite," *Sens. Actuators B, Chem.*, vol. 266, pp. 506–513, Aug. 2018.

[36] A. Lipatov, A. Varezhnikov, P. Wilson, V. Sysoev, A. Kolmakov, and A. Sinitskii, "Highly selective gas sensor arrays based on thermally reduced graphene oxide," *Nanoscale*, vol. 5, no. 12, pp. 5426–5434, Jun. 2013.

[37] H. Abunahla, Y. Halawani, A. Alazzam, and B. Mohammad, "NeuroMem: Analog graphene-based resistive memory for artificial neural networks," *Sci. Rep.*, vol. 10, no. 1, p. 9473, Jun. 2020.

[38] A. Agha et al., "A review of cyclic olefin copolymer applications in microfluidics and microdevices," *Macromolecular Mater. Eng.*, vol. 307, no. 8, Aug. 2022, Art. no. 2200053.

[39] A. Alazzam, "Solution-based, flexible, and transparent patterned reduced graphene oxide electrodes for lab-on-chip applications," *Nanotechnology*, vol. 31, no. 7, Feb. 2020, Art. no. 075302.

[40] A. Alazzam et al., "Transparent, patterned graphene oxide films with tunable electrical conductivity using thermal, chemical, and photoreduction techniques for lab-on-a-chip applications," *Anal. Bioanal. Chem.*, vol. 415, pp. 1339–1346, Jan. 2023.

[41] S. Rao, J. Upadhyay, K. Polychronopoulou, R. Umer, and R. Das, "Reduced graphene oxide: Effect of reduction on electrical conductivity," *J. Composites Sci.*, vol. 2, no. 2, p. 25, Apr. 2018.

Authorized licensed use limited to: TU Delft Library. Downloaded on January 03,2024 at 08:56:44 UTC from IEEE Xplore. Restrictions apply.

[42] T. F. Emiru and D. W. Ayele, "Controlled synthesis, characterization and reduction of graphene oxide: A convenient method for large scale production," *Egyptian J. Basic Appl. Sci.*, vol. 4, no. 1, pp. 74–79, Mar. 2017.
[43] F. Dawaymeh, Y. Abbas, M. Khaleel, A. Alazzam, and N. Alamoodi, "Tuning the surface wettability of cyclic olefin copolymer by plasma treatment and graphene oxide deposition and reduction," *Polymers*, vol. 13, no. 14, p. 2305, Jul. 2021.
[44] K. Humood, H. Abunahla, and B. Mohammad, "MemChar: Portable low-power and low-cost characterization tool for memristor devices," *IEEE Trans. Instrum. Meas.*, vol. 71, pp. 1–9, 2022.
[45] S. Kanan, O. El-Kadri, I. Abu-Yousef, and M. Kanan, "Semiconducting metal oxide based sensors for selective gas pollutant detection," *Sensors*, vol. 9, no. 10, pp. 8158–8196, Oct. 2009.
[46] P. Pal, A. Yadav, P. S. Chauhan, P. K. Parida, and A. Gupta, "Reduced graphene oxide based hybrid functionalized films for hydrogen detection: Theoretical and experimental studies," *Sensors Int.*, vol. 2, 2021, Art. no. 100072.
[47] L. S. K. Achary, B. Maji, A. Kumar, S. P. Ghosh, J. P. Kar, and P. Dash, "Efficient room temperature detection of H_2 gas by novel ZnFe2O4–Pd decorated rGO nanocomposite," *Int. J. Hydrogen Energy*, vol. 45, no. 7, pp. 5073–5085, Feb. 2020.
[48] V. Galstyan, E. Comini, I. Kholmanov, G. Faglia, and G. Sberveglieri, "Reduced graphene oxide/ZnO nanocomposite for application in chemical gas sensors," *RSC Adv.*, vol. 6, no. 41, pp. 34225–34232, 2016.
[49] J. Wang, B. Singh, S. Maeng, H.-I. Joh, and G.-H. Kim, "Assembly of thermally reduced graphene oxide nanostructures by alternating current dielectrophoresis as hydrogen-gas sensors," *Appl. Phys. Lett.*, vol. 103, no. 8, Aug. 2013, Art. no. 083112.
[50] A. Esfandiar, S. Ghasemi, A. Irajizad, O. Akhavan, and M. R. Gholami, "The decoration of TiO_2/reduced graphene oxide by Pd and Pt nanoparticles for hydrogen gas sensing," *Int. J. Hydrogen Energy*, vol. 37, no. 20, pp. 15423–15432, Oct. 2012.

Nada Abuhamra received the B.S. degree in electrical engineering from Abu Dhabi University, Abu Dhabi, UAE, in 2021, and the M.S. degree in electrical and computer engineering from the Khalifa University of Science and Technology, Abu Dhabi, in 2023, where she is currently pursuing the Ph.D. degree in electrical and computer engineering.

Heba Abunahla received the B.Sc. degree from United Arab Emirates University, Al Ain, United Arab Emirates, in 2007, the M.Sc. degree from the University of Sharjah, Sharjah, United Arab Emirates, in 2013, and the Ph.D. (Hons.) degree from Khalifa University, Abu Dhabi, United Arab Emirates, in 2017, via competitive scholarship.

She was an Assistant Professor and she had spent over five years as a Postdoctoral Fellow and a Research Scientist, working extensively on the design, fabrication, and characterization of emerging memory devices with great emphasis on computing, sensing, and security applications. She is currently an Assistant Professor with the Quantum and Computer Engineering Department, Delft University of Technology, Delft, The Netherland.

Dr. Abunahla received the Australian Global Talent Permanent Residency in 2021 for her achievements. She has several awards and competitive scholarships., e.g., she was a recipient of the Unique Fellowship for Top Female Academic Scientists—Electrical Engineering, Mathematics, and Computer Science from the Delft University of Technology in 2022. She serves as an Lead Editor in *Neuroscience* (Frontiers). She is an active reviewer for several high impact journals and conferences.

Ashraf Ali received the B.Sc. degree from The New College, University of Madras, Chennai, India, in 2005, the M.Sc. degree from the Jamal Mohammed College, Bharathidasan University, Tiruchirapalli, India, in 2007, the master's degree from the King's College London, London, U.K., in 2009, and the Ph.D. degree in material science from Anna University, Chennai, in 2019.

His expertise is in synthesis and characterization of polycrystalline and thin film materials for different applications. He is currently a Research Associate with the Emirates Centre for Energy and Environmental Research, United Arab Emirates University (UAEU), Al Ain, United Arab Emirates. His area of research focuses on the development of metal–oxide framework with conducting polymers for gas sensing applications.

Waqas Waheed received the Ph.D. degree in mechanical engineering from Khalifa University, Abu Dhabi, UAE, in 2019.

He is currently working as a Postdoctoral Fellow with the Microfluidics Laboratory, Khalifa University. His research interests include the development of microfluidic laboratory-on-a-chip platforms for biological applications and their numerical modeling using particle-based simulation methods, such as dissipative particle dynamics (DPD) and lattice Boltzmann methods (LBM).

Saleh T. Mahmoud received the Ph.D. degree in physics from the Indian Institute of Technology Delhi, New Delhi, India, in 2001.

He is a Full Professor with UAE University, Al Ain, United Arab Emirates, and has 20 years' experience in laser–plasma interactions, materials characterization, and nanodevices fabrication. His publication record includes about 82 publications in international peer-reviewed journals and more than 46 presentations in international conferences. He is the Principal Investigator and a Co-Principal Investigator of 23 research projects and supervised several postgraduate students. His research interests include phase-change materials for memory devices, synthesis of organic–inorganic hybrid materials for gas sensing applications, and nonlinear instabilities in laser plasmas.

Anas Alazzam is an alumnus of Concordia University, Montreal, QC, Canada. After a brief Postdoctoral Fellow appointment with the Canadian Space Agency, Longueuil, QC, Canada, he joined Khalifa University, Abu Dhabi, United Arab Emirates, in 2012, where he is currently an Associate Professor of Mechanical Engineering and the Head of the Microfluidics Laboratory. He has research background in microfluidics, nanofluids, dielectrophoresis, microsystems, phase change materials, and healthcare applications of microdevices.

Dr. Alazzam has received substantial recognition in the form of awards and media appearance for his research. He is a Editorial Board Member of the *Micromachines* and *PLOS One*.

Baker Mohammad (Senior Member, IEEE) received the B.S. degree in ECE from the University of New Mexico, Albuquerque, NM, USA, in 1994, the M.S. degree in ECE from Arizona State University, Tempe, AZ, USA, in 1998, and the Ph.D. degree in ECE from the University of Texas at Austin, Austin, TX, USA, in 2008.

He worked for ten years at Intel Corporation, Chandler, AZ, USA, with a focus on a wide range of microprocessors design from high performance, server chips $>$100 W (IA-64), to mobile embedded processor low power sub-1 W (Xscale). He was a Senior Staff Engineer or the Manager with Qualcomm, Austin, for six years, where he was engaged in designing high-performance and low-power DSP processors used for communication and multimedia application. He has over 16 years of industrial experience in microprocessor design, emphasizing memory, low power circuit, and physical design. He is the Director of the System-on-Chip Center and a Professor of EECS, Khalifa University, Abu Dhabi, United Arab Emirates. His research interests include very large-scale integration (VLSI), power-efficient computing, high-yield embedded memory, and emerging technology, such as memristor, STTRAM, and in-memory-computing, hardware accelerators for cyber-physical system. He is also engaged in a microwatt range computing platform for wearable electronics and WSN focusing on energy harvesting, power management, and power conversion, including efficient dc/dc and ac/dc converters. He has authored or coauthored over 150 referred journals and conference proceedings, more than three books, more than 18 U.S. patents, multiple invited seminars/panelists, and the presenter of more than three conference tutorials.

Authorized licensed use limited to: TU Delft Library. Downloaded on January 03,2024 at 08:56:44 UTC from IEEE Xplore. Restrictions apply.